Nematic liquid crystals in planar and cylindrical hybrid cells: Role of elastic anisotropy on the director deformations

R. T. Teixeira-Souza
Universidade Tecnológica Federal do Paraná, Campus Apucarana, Rua Marcílio Dias 635, 86812-460 Apucarana, Paraná, Brazil

C. Chiccoli and P. Pasini
Istituto Nazionale di Fisica Nucleare, Sezione di Bologna, Via Irnerio 46, 40126 Bologna, Italy

L. R. Evangelista
Departamento de Física, Universidade Estadual de Maringá, Avenida Colombo, 5790-87020-900 Maringá, Paraná, Brazil

C. Zannoni
Dipartimento di Chimica Industriale "Toso Montanari" and INSTM, Università, Viale Risorgimento 4, 40136 Bologna, Italy
(Received 13 April 2015; revised manuscript received 23 May 2015; published 1 July 2015)

Nematic samples filling a flat cell or the annular region between two concentric cylinders with hybrid anchoring conditions at the boundaries are investigated by setting up and minimizing their Frank elastic free energy. The coupling with the surfaces is taken to be strong on one side and weak on the other. The equations are numerically solved and the conditions for which the molecular organization inside the cell becomes uniform are analyzed. The classical calculation performed by G. Barbero and R. Barberi [J. Phys. **44**, 609 (1983)] is reproduced and investigated from a different point of view, in order to compare the results of planar and cylindrical geometries. The results suggest that the cylindrical cell presents some unusual features deserving a more complete investigation. Although most part of the transitional phenomena are found for $K_{11} > K_{33}$, a case not common for ordinary (lyotropic and thermotropic) liquid crystals, it is possible to find a completely uniform cell even for $K_{11} < K_{33}$ in both the geometries considered here.

DOI: 10.1103/PhysRevE.92.012501 PACS number(s): 61.30.Hn, 61.30.Gd

I. INTRODUCTION

One of the most attractive aspects of Liquid Crystals (LCs) is the possibility of creating and controlling specific molecular organizations with the use of external fields or even, when confining them at the micron scale, with suitable surface treatments. Amongst the LC features essential in determining the actual organization obtained, elasticity is crucial. Indeed, the elastic constants of splay, twist, and bend are key for the description of many phenomena in the physics of LCs [1–5], ranging from the formation and the topological charge of defects [6], the stability of blue phases [7], the sensitivity of biological sensors based on LCs [8], the pattern formations in chiral LCs [9], the stability of the bonded boojum-colloids in nematics [10], and many others. Here we are interested in LC in confined geometries and in the director deformations induced by the confinement produced by the surfaces, particularly in planar and cylindrical geometries when allowing for the difference in elastic constants. Although elastic constants K_{ii} are often found to be similar in many low-molar mass LC, justifying the common theoretical assumption of equal K_{ii}, large anisotropies were predicted by de Gennes for long molecules [11] and are found in a variety of materials [12]. When cylindrical samples are investigated considering the elastic anisotropy (i.e., when the elastic constants are allowed to be different), the non-usual deformations found [13–19] indicate that this kind of geometry can be more interesting than the planar one.

The aim of the present work is to investigate a nematic in an annular region between two concentric cylinders and the effects of the elastic anisotropy on the director orientation close to the surfaces for the cases of hybrid anchoring, i.e., of a strong anchoring on one side and a weak coupling on the other. We are also interested in studying the effects of tuning surface anchoring. Although this is difficult to realize experimentally, it could be achieved as shown for the case of LC droplets by using suitable mixtures of surface agents [20] or photoactive polymer surface coating [21]. The director angle is affected by the antagonistic alignment on the surfaces, for instance, when the alignment at the surface with strong anchoring is planar and the easy axis on the surface with weak anchoring is homeotropic. The particular case of one constant approximation in a planar geometry is a classical problem of elastic theory, that has been explored to get some information about the anchoring energy of the sample [2]. The anisotropic elastic case, partially reproduced here, was investigated many years ago by Barbero and Barberi [22] and is now analyzed here from a different perspective with the purpose of performing a comparison between the director behavior in planar and in cylindrical hybrid cells. More specifically the cylindrical cell considered here corresponds to the annular region between two concentric cylinders, filled with nematic liquid crystals. This case has been investigated in the one elastic approximation by means of elastic theory and Monte Carlo simulations in a previous work [23], where evidence was found of the importance of analyzing the effects of weak anchoring on both the inner and the outer surfaces clearly emerged.

The present paper is organized as follows. In Sec. II, the planar hybrid cell is investigated, the equation for the angle close to the surfaces as function of the parameters of the system

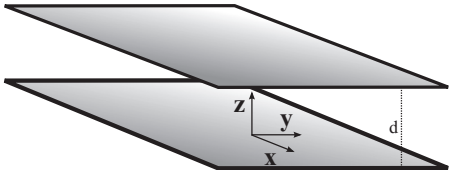

FIG. 1. Schematic representation of the planar sample with the surfaces placed at a distance d.

is obtained for the case of elastic anisotropy. The cylindrical case is investigated in Sec. III, where the equations and results are reported. Section IV is dedicated to a general discussion and to some concluding remarks.

II. THE HYBRID CELL: PLANAR GEOMETRY

A. Statement of the problem

The sample considered in this section consists of a nematic slab of thickness d along the z-axis, as illustrated in Fig. 1. The top and bottom surfaces, located at $z = \pm d/2$, are flat and considered to be infinite both in the x- and y-directions. The alignment at these surfaces is considered homogeneous, either homeotropic or planar (parallel to x). Under these assumptions, the director can be written as $\mathbf{n} = \sin\theta(z)\mathbf{i} + \cos\theta(z)\mathbf{k}$, with $\theta(z)$ denoting the angle between the director and the z-axis. An alignment parallel to $\mathbf{x}$ corresponds to $\theta = \pi/2$, while the alignment parallel to $\mathbf{z}$ corresponds to $\theta = 0$. The Frank expression of free energy may be written as

$$f_p = \frac{1}{4}K_{33}\int_V [k + 1 + (1-k)\cos 2\theta(z)]\,\theta'(z)^2\,dV \qquad (1)$$

with $\theta'(z) = d\theta/dz$ and $k = K_{11}/K_{33}$ defined as an elastic constant anisotropy parameter. It expresses the deviation from the common equal elastic constant approximation corresponding to $k = 1$. The usual procedure of minimizing the free energy yields the following non-linear Euler-Lagrange equation:

$$(k-1)\sin 2\theta(z)\theta'(z)^2 + [k + 1 + (1-k)\cos 2\theta(z)]\,\theta''(z) = 0, \qquad (2)$$

which can be rewritten in the form:

$$\theta'(z) = \frac{C_p}{\sqrt{[k + (1-k)\cos^2\theta]}}, \qquad (3)$$

where C_p is an integration constant. By considering that $\theta(\pm d/2) = \theta_{sb,a}$, where the indices b and a indicate the surfaces located at $z = +d/2$ and $z = -d/2$, respectively, it is possible to obtain an expression for the integration constant as

$$C_p = \frac{1}{d}\int_{\theta_{sa}}^{\theta_{sb}} \sqrt{[k + (1-k)\cos^2\theta]}\,d\theta. \qquad (4)$$

In this work, the cases in which the surfaces supply strong anchoring correspond to values of θ_{sa} and θ_{sb} which are 0 or $\pi/2$. However, in the cases in which the anchoring energy on the surface is finite, the values of the angle in the vicinity of the surface must be determined by taking into account the boundary conditions appropriate to the weak anchoring situation [2]. The anchoring energy expression considered here is the Rapini-Papoular one [24]:

$$f_s = -\tfrac{1}{2}W_{a,b}\cos^2(\theta_{sa,b} - \Theta_{a,b}), \qquad (5)$$

where W_i is the anchoring strength and Θ_i is the angle representing the easy direction, i.e., the angle which minimizes the anchoring energy in the absence of external effects. The boundary conditions can be written as

$$\pm 2L_{a,b}[k + (1-k)\cos^2\theta_{sa,b}]\,\theta'(z = \pm d/2) - \sin 2(\theta_{sa,b} - \Theta_{a,b}) = 0 \qquad (6)$$

with $L_i = K_{33}/W_i$ being an extrapolation length. By using the result of Eq. (3), it is possible to find that

$$\pm 2L_{da,b}\sqrt{[k + (1-k)\cos^2\theta_{sa,b}]} \times \int_{\theta_{sa}}^{\theta_{sb}} \sqrt{[k + (1-k)\cos^2\theta]}\,d\theta - \sin 2(\theta_{sa,b} - \Theta_{a,b}) = 0, \qquad (7)$$

where, for simplicity, we have introduced the scaled extrapolation length $L_{di} = L_i/d$. Equation (7) is numerically solved to yield the profiles of θ_{sa} and θ_{sb}, and, again by numerically solving Eq. (3), it is possible to obtain the profile of the director. Equation (7) can also be used to determine the critical values of k or L_{di} for which a completely uniform configuration is found ($\theta(z) = 0$ or $\theta(z) = \pi/2$), which is obtained when $\theta_{sa} \to \theta_{sb}$.

B. Results

Here we describe the various cases studied using the following concise notation where the two first letters refer to conditions on the surface located in $z = -d/2$ and the last two letters refer to the surface located at $z = +d/2$. The uppercase is used to indicate the alignment (X and Z for the slab and R and Z for the cylinder) and lowercase w,s to indicate the anchoring condition (w, weak or s, strong). The cases studied here are labeled as ZwXs and XwZs thus in essence we consider a case where the homeotropic aligning surface is weakly anchored and the planar strongly and vice versa.

The first case analyzed is the weak homeotropic, ZwXs, case and the results are shown in Figs. 2(a), 2(c). One notices that the larger the scaled extrapolation length L_d, e.g., because the film thickness d decreases for a given material, the greater the influence of the elastic anisotropy parameter k. In Fig. 2(a), the angle at the surface $z = -d/2$ is presented as a function of the scaled extrapolation length for some values of the elastic parameter k. The critical value of L_{da} for the transition from a deformed state to a completely uniform one ($\pi/2 - \theta_{sa} \to 0$) becomes higher if K_{11} is larger than K_{33}. In Fig. 2(b), the profile of $\pi/2 - \theta_{sa}$ as a function of the elastic parameter for some values of the scaled extrapolation length is shown. As expected, for $L_{da} = 1.0$, the critical value of k corresponds to the equal elastic constants case ($k = 1.0$). For cells with a weaker anchoring energy, the critical value of k tends to be smaller. To better understand this result, we plot the value of the scaled critical elastic parameter (defined as k_c) versus the scaled extrapolation length in Fig. 2(c). It is important to mention that, in this case, i.e., a very small value of $\pi/2 - \theta_{sa}$, the distortion corresponds to a small splay.

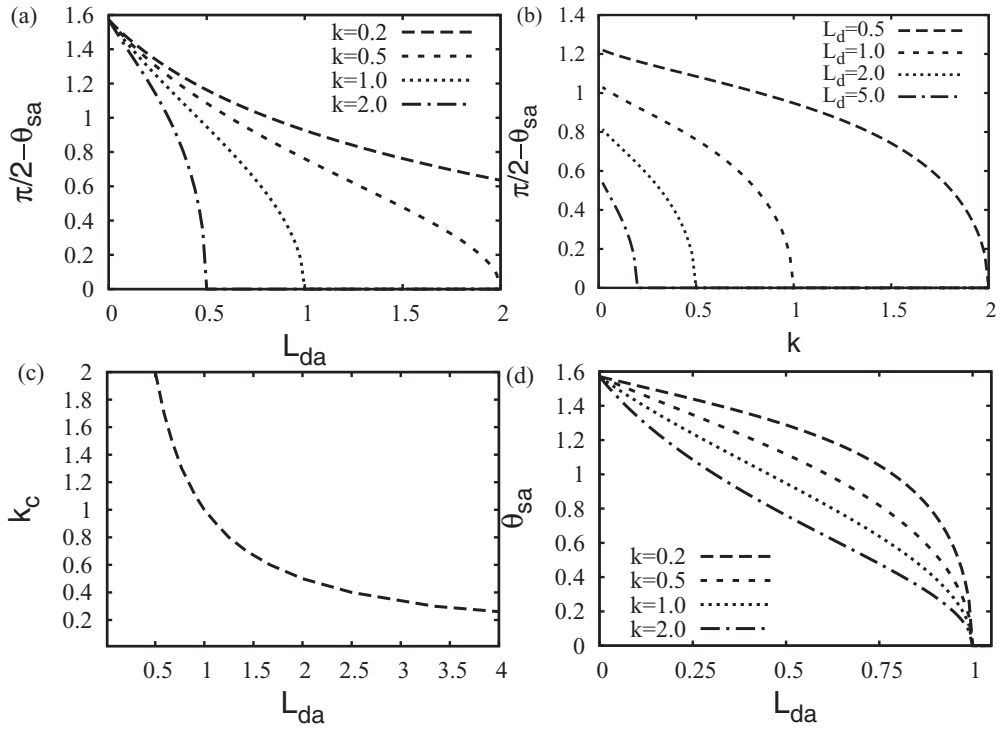

FIG. 2. The first three plates (a,b,c) refer to the ZwXs case. Anchoring angle at the surface located at $z = -d/2$ as a function of the scaled extrapolation length for a few values of the elastic constant parameter (a) and as function of the elastic anisotropy parameter for some values of the scaled extrapolation length (b); the dependence of the critical value of the elastic parameter on the scaled extrapolation length (c). The plate (d) shows the director angle close to the surface located in $z = -d/2$ versus the scaled extrapolation length for the XwZs case.

The profile of k_c as a function of L_{da} can be analytically determined from Eq. (7) by rewriting it as a power series in θ_{sa} around $\pi/2$ with $\theta_{sb} = \pi/2$ and $\Theta_a = 0$ up to third order. We then find

$$\frac{\pi}{2} - \theta_{sa} \approx \left\{ \frac{3(kL_{da} - 1)}{2[L_{da}(k-1) - 1]} \right\}^{1/2}, \tag{8}$$

yielding $\pi/2 - \theta_{sa} \to 0$ for $k_c = L_{da}^{-1}$ which coincides with the curve shown in Fig. 2(c) and implies $K_{11} = W_a d$, being the lowest value of splay elastic constant to get a homogeneous sample.

The XwZs case is quite different, as can be seen by looking at Fig. 2(d), where the profile of θ_{sa} is plotted against L_{da} for some values of the elastic parameter. The presence of elastic anisotropy affects the profile of θ_{sa} versus L_{da}, but the critical value does not change. This suggests that the elastic anisotropy parameter plays no role in the transition from a deformed to a uniform sample, for the XwZs case. Differently from the previous case, a small distortion corresponds to a very small bend deformation, and this case seems to be less sensitive to variations of the elastic parameter. If we now rewrite Eq. (7) as a power series of θ_{sa} around $\theta_{sa} = 0$, and again neglecting terms with order higher than three, with $\theta_{sb} = 0$ and $\Theta_a = \pi/2$, it is possible to obtain

$$\theta_{sa} \approx \left\{ \frac{2(1 - L_{da})}{3[L_{da}(k-1) + 1]} \right\}^{1/2}, \tag{9}$$

which yields $\theta_s \to 0$ if $L_{da} = 1$, or $K_{33} = W_a d$.

III. THE HYBRID CELL: CYLINDRICAL GEOMETRY

A. Statement of the problem

In this configuration the nematic sample is confined to the annular region between two concentric cylinders of radii r_1 and $r_2 > r_1$, as can be seen in Fig. 3. The length l_c of the cylinders is assumed to be long enough to be considered as infinite for our purposes. Since the alignments at the surfaces are considered as homogeneous planar (parallel to Z) or homeotropic (radial), the director can be written as $\mathbf{n} = \sin\phi(r)\mathbf{r} + \cos\phi(r)\mathbf{k}$, with ϕ being the angle formed by the director and the Z-direction.

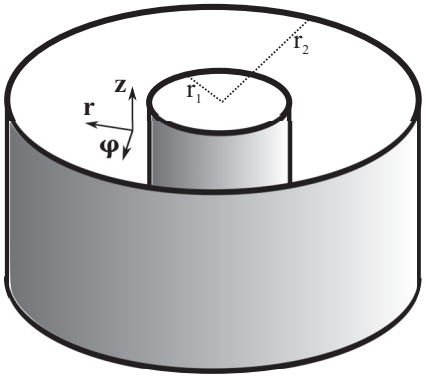

FIG. 3. A schematic representation of the annular region confined between two concentric cylinders and a sketch of the coordinates $\mathbf{r}$, $\boldsymbol{\varphi}$, and $\mathbf{z}$. The surfaces are placed at distances r_1 and r_2 from the center, with $r_2 - r_1 = d$.

The free energy, in this configuration, can be expressed as

$$f_c = \frac{1}{2}K_{33}\int_{V_c}\left\{k\frac{\sin^2\phi}{r^2} + [k+(1-k)\sin^2\phi]\phi'^2 + \frac{k\sin[2\phi]\phi'}{r}\right\}dV, \tag{10}$$

in which $k = K_{11}/K_{33}$ denotes an elastic anisotropy parameter, as before, and V_c is the volume of the cylindrical sample. By minimizing the free energy, it is possible to obtain the non-linear differential equation:

$$\frac{\sin 2\phi}{4}\left[2k-(1-k)\left(\frac{d\phi}{dx}\right)^2\right] - \frac{d^2\phi}{dx^2}[k+(1-k)\sin^2\phi] = 0 \tag{11}$$

with $x = \ln(r/r_1)$. Simple calculations allow us to simplify Eq. (11) to yield

$$\frac{d\phi}{dx} = \pm\sqrt{\frac{C_c + 2k\sin^2\phi}{\sin^2\phi + k\cos^2\phi}}, \tag{12}$$

where C_c is an integration constant to be determined. The anchoring energy is assumed to have the Rapini-Papoular form

$$f_s = -\tfrac{1}{2}W_{1,2}\cos^2(\phi_{s1,2} - \Phi_{1,2}),$$

with Φ_i being the angle corresponding to the easy axis, ϕ_i the actual angle at the surface, while the indices $i = 1,2$ refer at the surfaces with radii r_1 and r_2, respectively. By employing the boundary conditions suitable to weak anchoring, it is possible to find

$$C_c = -2k\sin^2\phi_{s1,2} + \frac{\{(r_{1,2}/2L_{1,2})\sin[2(\phi_{s1,2}-\Phi_{1,2})] + (k/2)\sin[2\phi_{s1,2}]\}^2}{\sin^2\phi_{s1,2} + k\cos^2\phi_{s1,2}}, \tag{13}$$

with $L_i = K_{33}/W_i$. By performing a separation of variables and an integration, from ϕ_{s1} to ϕ_{s2}, in Eq. (12) and using the integration constant obtained in Eq. (13), an expression for the angle on the surfaces can be obtained, namely,

$$\pm\int_{\phi_{s1}}^{\phi_{s2}} d\phi \sqrt{\frac{\sin^2\phi + k\cos^2\phi}{\frac{\{(r_{1,2}/2L_{1,2})\sin[2(\phi_{s1,2}-\Phi_{1,2})]+(k/2)\sin[2\phi_{s1,2}]\}^2}{\sin^2\phi_{s1,2}+k\cos^2\phi_{s1,2}} - 2k\sin^2\phi_{s1,2} + 2k\sin^2\phi}} - \ln\frac{r_2}{r_1} = 0. \tag{14}$$

Equation (14) is numerically solved for obtaining the angle at the surfaces and the set of values of the parameters for which a completely uniform state [$\phi(r) = 0$ or $\phi(r) = \pi/2$] is realized when $\phi_{s1} \to \phi_{s2}$.

B. Results

At a first glance it is possible to notice a crucial difference between Eqs. (14) and (7), which is key to distinguish the two geometries: it is the importance of the position of the surfaces in the equation. For the flat cell the two surfaces are perfectly equivalent and there is of course no difference if the planar alignment corresponds to the surface in $z = +d/2$ or $z = -d/2$, while in the present case the two surfaces belong to cylinders of different radii and have a different local curvature, so that this is a very important issue as also verified in [25]. Thus, we have analyzed all four combinations of weak and strong anchoring and planar and homeotropic boundary conditions, RsZw, RwZx, ZsRw, and ZwRs, for this geometry. Similar to the previous section, the first two letters denote the alignment and anchoring conditions at the outer surface (located at r_2) and the last two letters refer to the conditions at the inner surface (located at r_1). The four configurations were described in detail in Ref. [23]. The cases are investigated here by changing the extrapolation length, elastic parameter, and internal radius, while the external radius is kept fixed ($r_2 = 20$ units). We present results for the behavior of the angle at the surface with weak anchoring as a function of the extrapolation length, the internal radius, and the elastic anisotropy parameter k. Moreover, we show the critical value of the elastic parameter, k_c, as a function of the extrapolation length.

The results for the RsZw case are shown in Fig. 4. The profile of the angle at the surface analyzed for different values of the extrapolation length presents an interesting behavior [see Fig. 4(a)]: for surfaces with lower values of the extrapolation length (stronger anchoring) a higher value of k induces lower values of the angle at the surface. However, this behavior changes for the values of the extrapolation length higher than a certain value. In this case, it seems that the surface induces the reaching of the same angle, independently of the value of the elastic parameter. Then, the critical value of the extrapolation length is higher for higher values of the elastic parameter. When $\pi/2 - \phi_{s1}$ is investigated as a function of the inner cylinder radius, Fig. 4(b), it is possible to verify that for small values of the elastic constant, a uniform deformation is found for thicker samples (small r_1). In Fig. 4(c), we show the profile of the director angle at the surface as a function of the elastic parameter for some values of the extrapolation length. It is possible to verify that for a cell with weaker anchoring the elastic parameter must be higher to observe the completely uniform state. This result becomes more evident by looking at Fig. 4(d), where the critical value of the elastic parameter is plotted against the extrapolation length for a few values of the inner radius. In this plot, it is possible to see that, for samples with small value of the extrapolation length, the uniform deformation can be found for thinner samples (r_1 close to r_2).

A different behavior is manifested when the anchoring conditions are inverted, as can be seen in Fig. 5, for the RwZs case. In this case, the elastic parameter has a greater influence, as can be noticed from Figs. 5(a) and 5(b). Moreover, a lower value of the extrapolation length (higher values of anchoring energy) leads to a higher value of the critical value of the elastic parameter, as can be appreciated from Figs. 5(c) and 5(d).

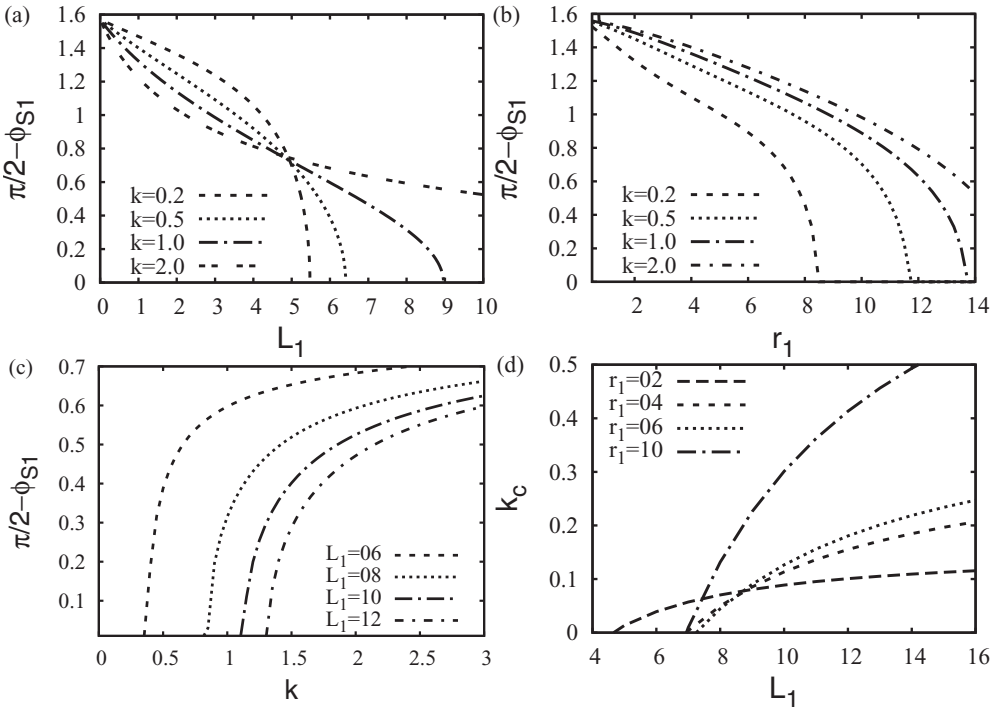

FIG. 4. RsZw case. Profile of $\phi_{s1} - \pi/2$ as function of L_1, for $r_1 = 14$ and a few values of the elastic parameters (a). $\phi_{s1} - \pi/2$ versus r_1 for $L = 10.0$ and a few values of the elastic parameter (b). The behavior of $\phi_{s1} - \pi/2$ as function of k for $r_1 = 14$ and some values of the extrapolation length (c). Critical values of the elastic parameter versus the extrapolation length, for some values of internal radio (d).

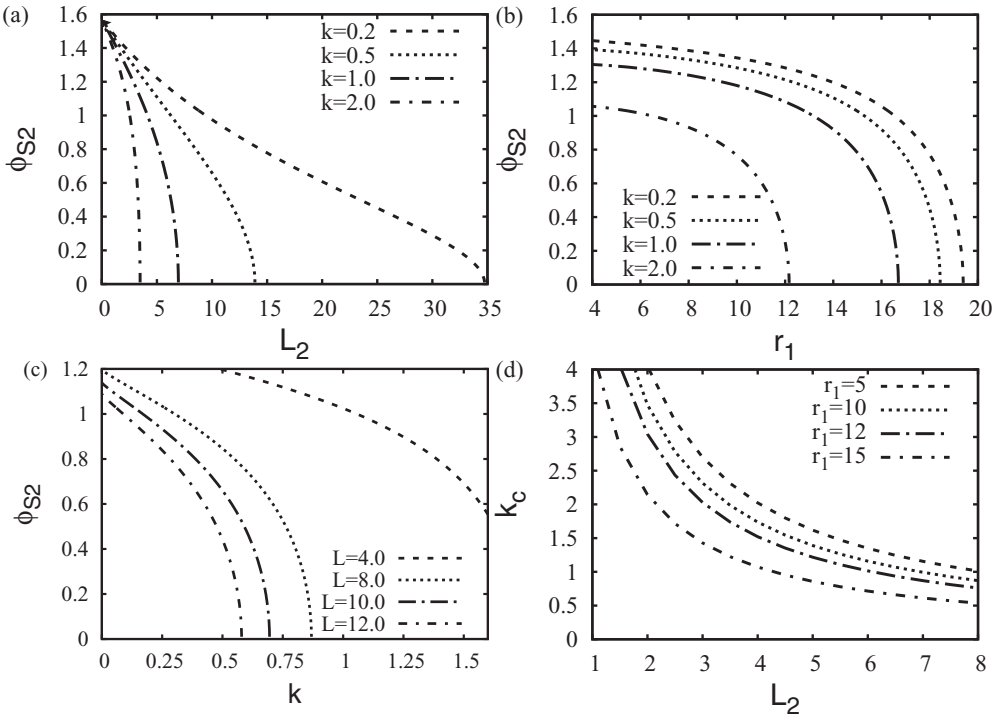

FIG. 5. RwZs case. The Profile of ϕ_{s2} is shown as function of L_2 (a), k (b), and r_1 (c). In (a) and (c) we have used $r_1 = 10$ and some values of the elastic parameter and extrapolation length, respectively, as indicated in the figure. In (b) the numerical calculation was performed for $L_2 = 3.0$ and a few values of the elastic parameter. The profiles of critical values of elastic parameter as function of the extrapolation length, for some values of the internal radius (d).

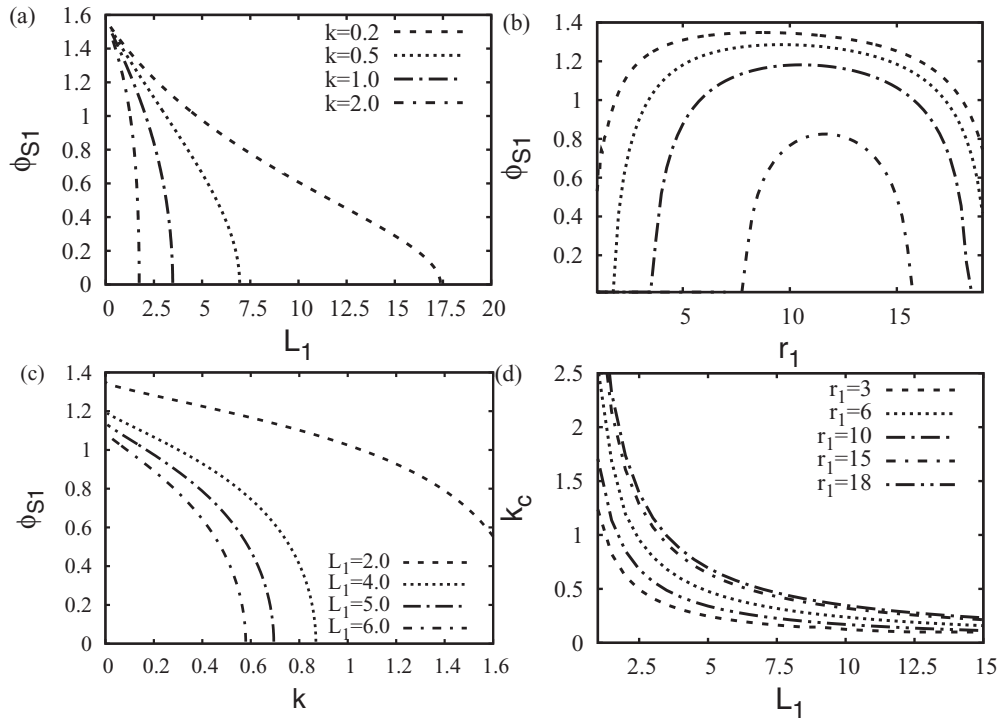

FIG. 6. ZsRw case. Profile of ϕ_{s1} as a function of L_1, for $r_1 = 10$, with some values of the elastic parameters (a), versus r_1 for $L_1 = 1.5$ and a few values of the elastic parameter (in which the line styles are the same used in (a)) (b) and as a function of k for $r_1 = 10$ and some values of extrapolation length (c). (d) As in Fig. 4(d).

The more interesting case is, however, the ZsRw one, whose results are shown in Fig. 6. The behavior of the angle at the surface is similar to the previous case, but the critical values of the extrapolation length are lower, due the weak anchoring with the inner surface. Besides, as discussed also in [23], the external surface alignment is more effective and the alignment parallel to Z is energetically preferred. In this case, these two situations become competitive, which can explain the non-monotonic behavior of the angle at the surface as a function of the inner cylinder radius, see Fig. 6(b). The results for the angle at the surface versus elastic parameter for few values of extrapolation length are presented in Fig. 6(c). The profiles of the critical elastic parameter as function of the extrapolation length, Fig. 6(d), also show an interesting behavior for the various values of inner radius. Note that the curves for $r_1 = 3$ and $r_1 = 18$ are very close (respectively, the lowest and the highest values for inner surface radius investigated).

Finally, the results of the last case (ZwRs) are shown in Fig. 7. Although the behavior seems very similar to the RsZw case, some important differences emerge. The main difference is in the extrapolation length values required to observe the uniform state, see Fig. 7(a). In both cases, however, the profile of $\pi/2 - \phi_{s2}$ as function of k and the behavior of the angle as a function of the inner surface radius become close to that of a uniform state. When we have a weak coupling at the inner surface, the anchoring energy must be lower than the opposite case. Moreover, a change in the sample thickness does not seem to affect the angle in the vicinity of the surface, for values close to the easy axis direction and, consequently, the profile of the director. It will be more relevant close to the conditions for uniformity, which also changes a little with the elastic parameter, as observed in Fig. 7(b).

In the limit $r_{1,2} \to \infty$, with the difference $(r_2 - r_1 = d)$, the curvature of the cylinders becomes very small and the sample behavior could be similar to that of a slab. Thus, we can assume $\ln(r_2/r_1) \approx d/r_{1,2}$, and the Eq. (14) can be written

$$\frac{1}{\sqrt{\frac{(r_{1,2}/2L_{1,2})^2 \sin^2[2(\phi_{s1,2}-\Phi_{1,2})]}{\sin^2\phi_{s1,2}+k\cos^2\phi_{s1,2}}}} \times \int_{\phi_{s1}}^{\phi_{s2}} d\phi \sqrt{\sin^2\phi + k\cos^2\phi} - \frac{d}{r_{1,2}} = 0, \quad (15)$$

which provides the same numerical results of Eq. (7).

IV. DISCUSSION AND CONCLUDING REMARKS

We have examined the possibility of tuning the director deformations in flat or cylindrical hybrid cells by varying surface anchoring from weak to strong and easy axis from planar to homeotropic, paying particular attention to the role of elastic constants anisotropy. As observed in both the geometries, the elastic anisotropy in a hybrid cell strongly affects the behavior of the director angle close to the surface. In the slab case, a planar or homeotropic orientation on the surface with strong anchoring shows a very different behavior, which is not the case for the one elastic constant approximation often used. The curvature and the different size of the surfaces, however, introduce some interesting peculiarities for the cylindrical sample. Besides that, in this kind of geometry, the elastic anisotropy presents a much

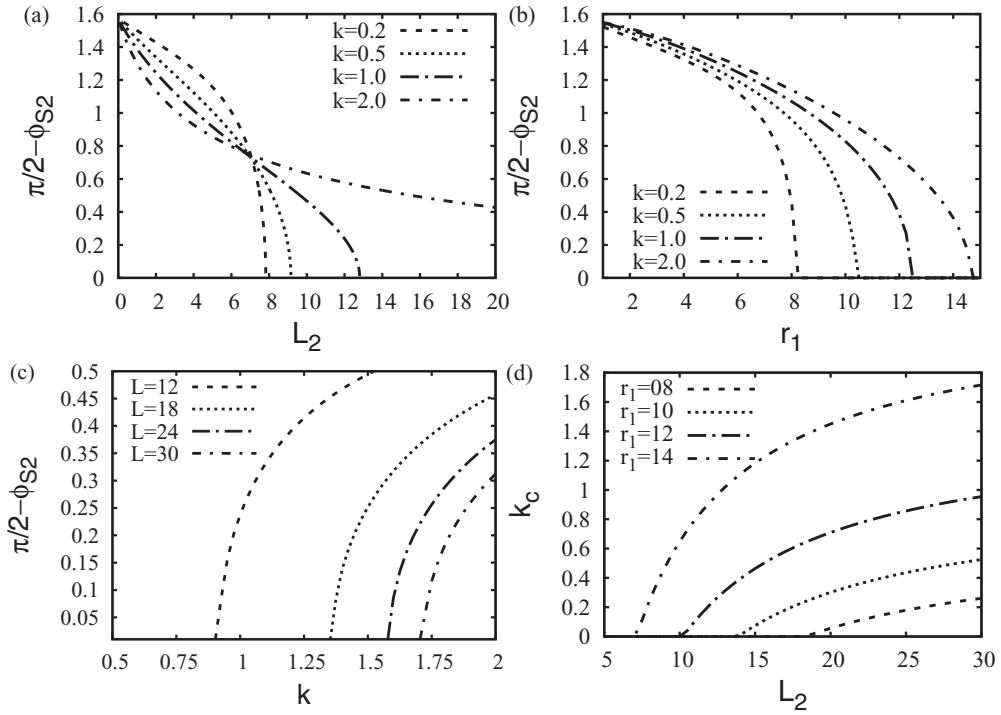

FIG. 7. ZwRs case. Results of the numerical analysis of $\phi_{s2} - \pi/2$ as function of L_2, for some values of the elastic parameters (a). Profile of $\phi_{s2} - \pi/2$ versus r_1 for $L_2 = 20.0$ and a few values of the elastic parameter (b). (c) $\phi_{s2} - \pi/2$ versus k for a few values of extrapolation length. In both cases (a) and (c) we have used $r_1 = 14$. (d) As described in Fig. 4(d).

more complex behavior than the one observed in a planar geometry. Even in the most similar case, where the alignment with strong anchoring is parallel to Z and one would expect a similar behavior of the orientation close to the surface, some differences emerge. In particular at the threshold where the cell becomes completely uniform, a small distortion in the radial direction close to the surface with weak anchoring still affects the orientation of the director. An important issue to be noticed is that, for lyotropic and thermotropic liquid crystals, there is a large variability of the elastic anisotropy parameter. The results presented here thus offer a rather general solution allowing reasonable estimates, even for non intuitively obvious cases, of the director deformations for the full range of elastic anisotropies.

ACKNOWLEDGMENTS

R.T.T-S. and L.R.E. are grateful to Brazilian agencies CAPES and CNPq (Grant No. 443339/2014-7) for financial support.

[1] P. G. de Gennes, *The Physics of Liquid Crystals* (Oxford Press, London, 1974).
[2] G. Barbero and L. R. Evangelista, *An Elementary Course on the Continuum Theory for Nematic Liquid Crystals* (World Scientific, Singapore, 2001).
[3] I. W. Stewart, *The Static and Dynamical Continuum Theory of Liquid Crystals* (Taylor & Francis, London, 2004).
[4] W. H. de Jeu, Mol. Cryst. Liq. Cryst **63**, 83 (1981).
[5] M. Buscaglia, G. Lombardo, L. Cavalli, R. Barberi, and T. Bellini, Soft Matter **6**, 5434 (2010).
[6] For example, C. Chiccoli, P. Pasini, R. Teixeira de Souza, L. R. Evangelista, and C. Zannoni, Int. J. Mod. Phys. C **22**, 505 (2011), and references therein.
[7] J. I. Fukuda, Phys. Rev. E **85**, 020701 (2012).
[8] W. Iglesias, N. L. Abbott, E. K. Mann, and A. Jákli, Appl. Mater. Interfaces **4**, 6884 (2012).
[9] R. S. Zola, L. R. Evangelista, Y.-C. Yang, and D.-K. Yang, Phys. Rev. Lett. **110**, 057801 (2013).
[10] Z. Eskandari, N. M. Silvestre, and M. M. Telo da Gama, Langmuir **29**, 10360 (2013).
[11] P. G. de Gennes, Mol. Cryst. Liq. Cryst. Lett. **34**, 177 (1977).
[12] C. Chiccoli, P. Pasini, and C. Zannoni, Mol. Cryst. Liq. Cryst. **516**, 1 (2010), and references therein.
[13] H. Tsuru, J. Phys. Soc. Jpn. **59**, 1600 (1990).
[14] D. R. M. Williams and A. Halperin, Phys. Rev. E **48**, R2366 (1993).
[15] D. R. M. Williams, Phys. Rev. E **50**, 1686 (1994).
[16] A. Corella-Madueño, A. Castellanos-Moreno, S. Gutierrez-Lopez, R. A. Rosas, and J. A. Reyes, Phys. Rev. E **78**, 022701 (2008).
[17] R. Teixeira de Souza, J. C. Dias, R. S. Mendes, and L. R. Evangelista, Physica A **389**, 945 (2010).
[18] C. Chiccoli, P. Pasini, L. R. Evangelista, R. T. Teixeira-Souza, and C. Zannoni, Phys. Rev. E **91**, 022501 (2015).
[19] B.-J. Liang and Shu-Hsia Chen, J. Appl. Phys. **71**, 2189 (1992).

[20] G. E. Volovik and O. D. Lavrentovich, Zh. Eksp. Teor. Fiz. **85**, 1997 (1983) [JETP **58**, 1159 (1983)].

[21] V. Chigrinov, in *Liquid Crystal Devices Based on Photoalignment and Photopatterning Materials* in *Emerging Liquid Crystal Technologies IX Book Series*, edited by L. C. Chien, A. M. F. Neto, K. Neyts *et al.* [Proc. SPIE **9004**, 90040A (2014)].

[22] G. Barbero and R. Barberi, J. Phys. **44**, 609 (1983).

[23] C. Chiccoli, P. Pasini, L. R. Evangelista, R. Teixeira de Souza, and C. Zannoni, Mol. Cryst. Liq. Cryst. **576**, 42 (2013).

[24] A. Rapini and M. Papoular, J. Phys. Colloq. (Paris) **30**, C4-54 (1969).

[25] C. Chiccoli, P. Pasini, R. Teixeira de Souza, L. R. Evangelista, and C. Zannoni, Phys. Rev. E **84**, 041705 (2011).